Journal of the European Ceramic Society 19 (1999) 441–449

PII: S0955-2219(98)00214-3
0955-2219/99/$—see front matter

Quantitative Evaluation by Fractal Analysis of Indentation Crack Paths in Si_3N_4–SiC_W Composites

Annamaria Celli, Antonella Tucci* and Leonardo Esposito

Italian Ceramic Center, Via Martelli 26, 40138 Bologna, Italy

(Received 13 March 1998; accepted 29 April 1998)

Abstract

The crack paths, generated by Vickers indentation in Si_3N_4–SiC_w composites, were analysed from a quantitative point of view, in order to distinguish between the possible toughening mechanisms involved. It was found that the roughness parameter R_L *and the fractal dimension* D *describe the geometrical features of the cracks and evidence the anisotropy of the microstructure, due to the whisker and Si_3N_4β-grain orientation. The relationships found between fracture toughness and these geometrical parameters emphasise the importance of the crack deflection mechanism in improving toughness and provide information on the role played by microstructure in determining the mechanical properties of a composite.* © *1999 Elsevier Science Limited. All rights reserved*

Keywords: Si_3N_4, SiC, whiskers, fractal analysis, toughness and toughening.

1 Introduction

Fractal geometry, developed by Mandelbrot in 1977,[1] has been successfully used to describe quantitatively complex shapes such as fracture surfaces in metal,[2] ceramic[3,4] and polymeric[5] materials. This description is based on the assumption that crack propagation in materials is a fractal process and the crack surface presents a self-similar property, i.e. its shape is statistically invariant under isotropic scale transformations. This fractal approach, widely discussed[6–9] after the first works of Mandelbrot, represents a new way to quantitatively characterise the topography of a surface and to avoid the influence of the magnification used in obtaining fractographic data.[10,11] A concept such as roughness, which is sensitive to magnification, is replaced by an exponent that refers not to the roughness itself, but to the way in which the roughness changes when the observation scale changes. For a fracture surface, for example, this exponent is the fractal dimension D, a scale invariant parameter which varies between 2 and 3 as a function of the geometrical complexity of the system.

Fracture surface analysis, by fractal geometry, has been applied to distinguish the geometrical effects of different fracture mechanisms. For several ceramic materials, a direct correlation between fracture toughness K_{IC}, and the fractional part of the fractal dimension D^*, has been found[3,4,12]:

$$K_{IC} = K_0 + AD^{*0.5}$$

where A is a constant for classes of materials characterised by the same microstructural features. The A value can be related to the fracture mechanism at the atomic level and suggests some interesting relationships between microstructure and toughness.

The present study involved the investigation of fracture processes by analysing the geometry of crack profiles instead of fracture surfaces. The crack paths generated in different Si_3N_4–SiC_w composites were analysed in order to obtain information about the toughening mechanisms involved. It is well known that the fracture toughness and strength of Si_3N_4 ceramics can be increased by the addition of whiskers.[13,14] The resulting toughening effect is due to crack deflection, bridging of whiskers, debonding and pull-out as well as residual stresses caused by thermal expansion mismatch.[14–16] The toughness of these materials then is closely related to their microstructural features. Since fractal analysis allows one to quantify crack roughness, it was possible to evaluate the contribution of the crack deflection mechanism in controlling crack propagation and to

*To whom correspondence should be addressed. Fax: + 39-51-53-00-85

study the relationship between microstructure and mechanical properties.

Finally, the crack parameters were extrapolated to the corresponding fracture surface parameters[17,18] in order to compare them with those reported in literature for other materials.[3,4]

2 Experimental Part

Four samples of Si_3N_4 containing 0, 5, 10 and 20% of SiC whiskers prepared by hot-pressing[19] were analysed. For each composite, two surfaces, perpendicular and parallel to the hot pressing direction, were cut and polished in order to obtain two series of three samples each. For the Si_3N_4 sample, only the surface perpendicular to the hot pressing direction was considered.

The cracks, obtained by Vickers indentation with a load of 98·1 N, were observed with a scanning electron microscope, SEM. The corresponding micrographs all taken at the same magnification, were elaborated by image analysis and their profiles were digitised. The fracture toughness K_{IC}, was determined using the Vickers indentation technique and the Anstis equation.[20]

3 Theoretical Background

3.1 Analysis of a profile

A fractal object is characterised by a dimension that could be a fractional number, included between the Euclidean dimension of the object and the dimension of the space where the object itself is embedded. The fractal dimension of an irregular curve, such as a crack, has a value between 1 and 2, depending on the shape and geometry of the curve. The problem of how to determine this number was first discussed by Mandelbrot,[1,21] who observed that when the magnification is increased or the size of the measuring unit decreased, the length of an irregular curve increases without limit. This effect is described by the following equation:

$$L(\eta) = L_0 \eta^{-[D-1]} \tag{1}$$

where L is the real length, L_0 is a constant with dimension of L, η is the size of the measuring unit and D, varying between 1 and 2, represents the fractal dimension of the curve. $(D-1) = D^*$ is the fractional part of the fractal parameter of the irregular profile. The linear form of eqn (1) is:

$$\ln L(\eta) = \ln L_0 - (D-1)\ln \eta \tag{2}$$

The parameter D can be obtained from the slope of the straight line obtained in the plot $\ln L(\eta)$ versus $\ln \eta$, known as Richardson plot.

Often, the linearity predicted by eqn (2) is not observed; L is expected to increase without limit for $\eta \to 0$, while it tends to a limit value for small values of η. Underwood *et al.*[17,18] discussed the problem of how to linearize this plot. They used the term $R_L = L/L'$, where L is the real length of the irregular curve and L' is the projected length. This term represents the tortuosity of the irregular profile and is useful in order to compare the length of different objects. The dependence of R_L on η has the same form as eqn (1), dividing both sides of eqn (1) by L':

$$R_L(\eta) = R_{L0} \eta^{-[D-1]} \tag{3}$$

that in the logarithmic plot often shows a reversed sigmoidal trend. The linearization of this plot was obtained by Underwood[17] and co-workers with the following expression:

$$\log\log\left[\frac{(R_L)_0 - (R_L)_\infty}{R_L(\eta) - (R_L)_\infty}\right] = \log\left(\frac{\alpha}{2{\cdot}3}\right) \pm \beta \log \eta \tag{4}$$

where $(R_L)_0$ and $(R_L)_\infty$ represent the asymptotes as $\eta \to 0$ and $\eta \to \infty$ respectively; α and β are constants. $D_\beta = \beta + 1$ is the new fractal parameter proposed by the authors and is more effective than the conventional fractal parameter D, to describe the geometry of an irregular curve.

Because the experimental data obtained in this work show a sigmoidal trend in the plot $\log R_L$ versus $\log \eta$ and not versus η, as eqn (4) requires, an alternative approach was adopted. A slightly different equation is proposed to determine the fractal parameter of an irregular profile, based on the general equation describing a reversed sigmoidal curve:

$$y = \exp[-kx^n] \tag{5}$$

where y varies between 0 and 1, k is a constant and n is the fractal parameter correlated to the geometry of the object analysed. The idea that n is a fractal parameter is suggested by studies on the relaxation kinetics of thermodynamic properties described by equations similar to eqn (5) where the n exponent, a fractal coefficient,[22] varies between 0 and 1. The linearization of eqn (5) is obtained by eqn (6) that allows a straight line to be obtained, the intercept of which is $\log k'$ and the slope of which is n

$$\log(-\log y) = \log k' + n \log x \tag{6}$$

For the present case, y corresponds to $\log R_L(\eta)$ and x to $\log \eta$. Because the values of y have to vary between 0 and 1, it is necessary to divide $\log R_L(\eta)$ by $\log(R_L)_0$, where $\log(R_L)_0$ represents the asymptotic value of $\log R_L(\eta)$ when $\log \eta \to 0$. The following linear equation is obtained:

$$\log\left[-\log\frac{\log R_L(\eta)}{\log(R_L)_0}\right] = \log K' + n\log(\log \eta) \quad (7)$$

where n lower than 1, represents the fractional part of the fractal parameter. The fractal dimension of the irregular curve called D_n, is obtained by adding 1 (the Euclidean dimension of a line) to the n value. In order to compare the parameter D_n, to the 'classical' fractal dimension D, we also tried to obtain the D values by linear regression analysis of the plots of $\log R_L(\eta)$ versus $\log \eta$ using the central portion of each curve.

The experimental data required to apply the eqn (7) are the values of L for different η values; they were calculated by the application of the dividers technique.[23] By changing η, different polygonal approximations of the profile are obtained. Their total length L, can be calculated by adding the distances from point to point, with the Pythagorean rule:

$$L = \sum_{i=n}^{n} \sqrt{(x_i - x_{i-1})^2 + (y_i - y_{i-1})^2} \quad (8)$$

where the index i counts through the list of points. Equation (8) shows that the minimum distance between two points in the x-axis is equal to $(x_i - x_{i-1})$ and is the smallest size of the measuring unit η. When i-1 is substituted for i-2 in eqn (8), η doubles and L decreases. If the procedure is repeated by substituting $i-1$ for $i-3$, $i-4$ etc., the length L continues to decrease and the values of L as a function of η are obtained. When the $n-$th point is used for the calculation of L, it is possible to choose between n different starting points x_n, each of which gives a slightly different total length. For this reason the calculation of $L(\eta)$ was made for every possible starting point and the final $L(\eta)$ value is an average of all the $L(\eta)$ data. This improves the precision of the resulting fit.[24]

3.2 Fracture surfaces

A fractal surface is characterised by a dimension varying between 2 and 3 depending on its complexity. Many experimental methods have been developed to determine the fractal dimension of a surface by analysing directly fracture surfaces of both metals and ceramics.

Also several analytical methods have been proposed to determine the fractal dimension of a surface, based on a knowledge of the corresponding roughness parameter of a curve, R_L. These methods have been applied when vertical sections through the fracture surface were analysed.[11,17,18] Directly from R_L by using a linear parametric equation, it is possible to calculate the corresponding surface parameter R_S, defined as the ratio between the real surface area $S(\eta^2)$ divided by its projected area. The equation that provides the best fit of all known experimental data is:[11]

$$R_s = \frac{4}{\pi}(R_L - 1) + 1 \quad (9)$$

where R_s represents the surface roughness. The dependence of R_s from η^2 is based on the fractal characteristics of the surface. By analogy to the profile of a curve, an equation similar to eqn (7) was found in order to determine the fractal exponent:

$$\log\left[-\log\left(\frac{\log R_s(\eta^2)}{\log(R_s)_0}\right)\right] - \log K'' + n_s \log\log(\eta^2) \quad (10)$$

where $\log(R_S)_0$ represents the asymptotic value of $\log R_S(\eta^2)$ when $\log(\eta^2) \to 0$; n_S varies between 0 and 1 and represents the fractal characteristics of surfaces. This fractal analysis procedure can be applied to the crack path, if it is assumed that the geometrical characteristics of the crack profile can be extrapolated to three-dimensionality and correspond to the geometrical characteristics of the hypothetical fracture surface obtained in the bulk sample. This extrapolation corresponds to a passage from a fractal dimension between 1 and 2 (irregular curve) to a fractal dimension between 2 and 3 (irregular surface). In this way it is possible to compare the experimental data obtained in the present study with those reported in literature for fractal surfaces.

4 Results and Discussion

4.1 Analysis of the crack geometry

Whisker orientation during hot-pressing of ceramic composites, leads to anisotropy in both the morphology and mechanical properties of the composites.[13,25] In the plane perpendicular to the hot-pressing direction, the whiskers are essentially randomly oriented with their axis parallel to the plane (Fig. 1, case a). The interaction between whiskers and growing cracks is random and isotropic, consequently $1_\perp$ and $2_\perp$ type cracks have similar lengths and shapes. In the plane parallel to the hot-pressing direction, whiskers show either their sections or their axes aligned perpendicularly

to the hot-pressing direction, (Fig. 1, case b). As a consequence, type $1_{//}$ cracks are shorter than type $2_{//}$ cracks. It should be pointed out that X-ray diffraction patterns indicate, according to the procedure suggested by Lange,[26] that also the elongated β-grains showed a preferred orientation perpendicular to the hot-pressing direction in all the samples tested. The orientation of these grains together with the distribution of the whiskers influence the degree of crack deflection according to the plane where the crack is analysed. In order to emphasise this effect on the length and shape of a crack, for the samples tested, differently oriented cracks with respect to the pressing direction, crack types $1_{\perp}$, $2_{\perp}$, $1_{//}$ and $2_{//}$ were analysed separately. The aim of this analysis was to study the average tendency of a crack to present a particular path geometry rather than another one and to try to explain this characteristic with microstructural considerations.

Reported in Table 1 are the $(R_L)_0$ values, extrapolated to $\eta \to 0$, for the samples analysed in the three different orientations. This roughness parameter can suggest some quantitative indications about the crack tortuosity. The Si_3N_4 sample without whiskers is characterised by a low $(R_L)_0$ value, due to a quasi-linear crack path. The presence of a low degree of crack deflection depends on the grain shape and on the intergranular fracture behaviour.[13] In the plane perpendicular to the hot-pressing axis, the effect of the presence of whiskers is evident in the increase of path tortuosity for the composites, even though the random and not very high values of $(R_L)_0$ for crack types $1_{\perp}$ and $2_{\perp}$ are probably due to a disordered disposition of whiskers on the surface. The most important effect of the presence of whiskers is evident for crack type $1_{//}$ in the plane parallel to the hot-pressing axis, where the highest $(R_L)_0$ values for every whisker percentage are due to the β-Si_3N_4 grain alignment and whisker orientation. SEM micrographs show that the cracks are usually deflected by whiskers, placed perpendicularly to the direction of crack growth, causing a very rough path, Fig. 2 (a). This effect is particularly significant for a whisker percentage of 20%, which leads to a considerable increase in path tortuosity. On the other hand, the influence of whisker

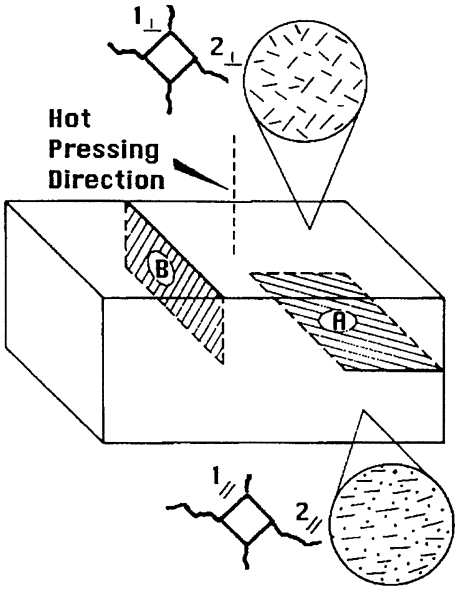

Fig. 1. Schematic representation of the whiskers orientation in a hot pressed sample (Ref. 25).

Table 1. Roughness parameter $(R_L)_0$ calculated for the different types of cracks

Whisker content %	$(R_L)_0$		
	Crack types $1_{\perp}$ *and* $2_{\perp}$	*Crack type* $1_{//}$	*Crack type* $2_{//}$
0	1·17	–	–
5	1·26	1·25	1·24
10	1·15	1·40	1·24
20	1·48	1·72	1·30

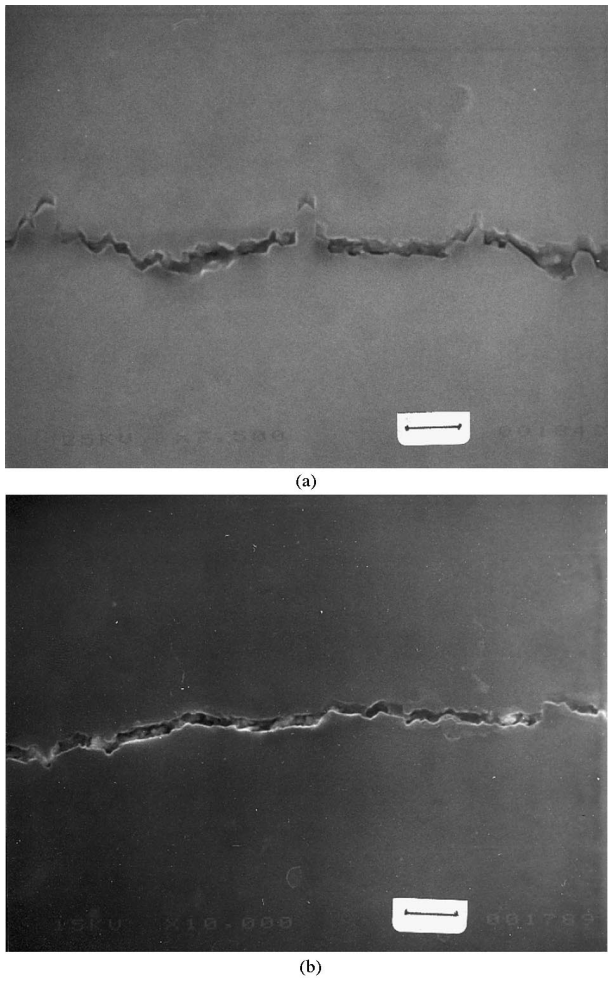

Fig. 2. SEM micrographs of crack profiles in the Si_3N_4–10% SiC_w sample: (a) crack type $1_{//}$, the bar is 1·3 μm, and (b) crack type $2_{//}$, the bar is 1 μm.

percentage on the tortuosity of crack path and, then, on the degree of crack deflection is not very significant for type $2_{//}$ cracks, with the exception of the composite with 20% of whiskers. These cracks are parallel to the whisker axis and tend to go straight on, following the whisker edge with a mechanism that does not cause a very rough path, Fig. 2 (b).

The plot of $\log R_L(\eta)$ versus $\log(\eta)$ is a sigmoidal curve and its linear extrapolations provide the fractal parameters D and D_n. Figure 3 shows that D increases linearly with increasing $(R_L)_0$, independently of the sample composition, the plane containing the crack and the whisker orientation. Therefore, D is a measure of the roughness of the crack path.

Differently, the dependence of D_n on $(R_L)_0$ varies according to the kind of crack, Fig. 4. D_n is nearly constant for type $1_\perp$ and $2_\perp$ cracks, with the exception of the Si_3N_4 sample without whiskers. For the other cracks, D_n increases with increasing $(R_L)_0$, but with a different trend. Thus, D_n has a more complex dependence on crack geometry than D and seems to be able to differentiate between cracks obtained in different conditions with regard to indentation plane and whisker orientation. This is the same result obtained by Underwood and coworkers[17,18], who show that their new fractal parameter D_β calculated using eqn (4), presents a different dependence, with respect to R_L, R_s and D, from the tempering temperature for their samples.

To obtain a better understanding of this result, crack profiles were analysed according to their geometric characteristics. The average number of the crack deflections per unit length, the average length of the linear segments and the deflection angles were measured. The average length of the rectilinear segments l, was evaluated by counting the average number of deflections d, that the crack showed along its path L' and by dividing the real crack length L by this number, Table 2.

Figure 5 shows the percent frequency of deflection angles in the range from 0 to 100° for the sample containing 5% whiskers and analysed in the three different directions. From the results of Table 2 and Fig. 5, type $1_\perp$ and $2_\perp$ cracks are characterised by a high percentage of low deflection angles, included between 0 and 20°, by a large number of deflections along the path and by short linear segments. This kind of trajectory induces relatively low values of $(R_L)_0$. Cracks of the type $1_{//}$, on the contrary, show a significantly high percentage of deflection angles in the range of 60°, a low number of deflections, long linear segments and then, high $(R_L)_0$ values. For type $2_{//}$ cracks there are a high percentage of deflection angles in the range of 40° and long linear segments, but the path tortuosity does not change with the whisker percentage.

In conclusion, cracks appear to be geometrically different depending on the whisker orientation. The fractal parameter D_n allows one to distinguish different crack profiles on the basis not only of their roughness but also of their particular geometry.

4.2 Correlation between fractal parameters and fracture toughness

Since the fracture toughness is calculated from the length of the cracks emerging from the Vickers impressions, it is reasonable that the calculated K_{IC} values are influenced by the anisotropy of the materials. The fracture toughness increases as the percentage of whiskers increases, in particular for type $1_{//}$ cracks, as reported in literature[13,25]

The values of K_{IC} are reported in Fig. 6 as a function of the fractal parameter D. Two different behaviours can be identified. In general, for type $1_\perp$ and $2_\perp$ cracks, in the plane perpendicular to the hot-pressing direction, K_{IC} does not change as a function of D, with the exception of the sample Si_3N–4 20% SiC_w. Instead, the toughness increases linearly with increasing D for type $1_{//}$ cracks and,

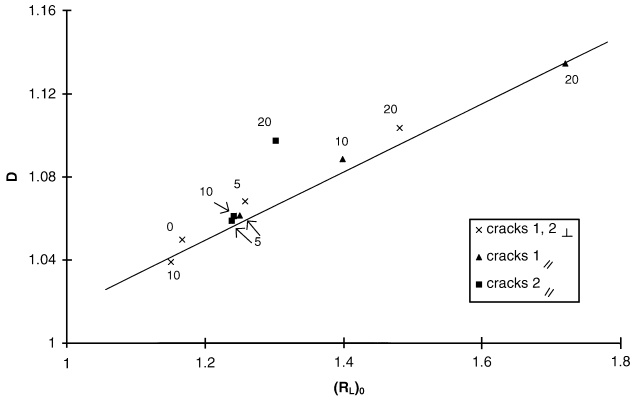

Fig. 3. Fractal parameter D as a function of the roughness parameter $(R_L)_0$. The numbers in the plot represent the percentage of whiskers in the samples.

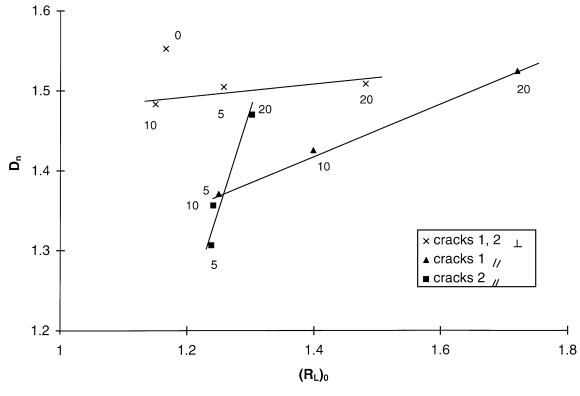

Fig. 4. Fractal parameter D_n as a function of the roughness parameter $(R_L)_0$. The numbers in the plot represent the percentage of whiskers in the samples.

Table 2. Average number of crack deflections per unit length, *d*, and average length of the linear segments, *l*, calculated for the different types of cracks

Whisker content %	d (μm^{-1})			l (μm)		
	Crack types $1_\perp$ *and* $2_\perp$	*Crack type* $1_{//}$	*Crack type* $2_{//}$	*Crack types* $1_\perp$ *and* $2_\perp$	Crack type $1_{//}$	Crack type $2_{//}$
0	3·05	–	–	0·38	–	–
5	4·61	2·74	2·49	0·31	0·46	0·50
10	4·57	2·68	2·47	0·30	0·51	0·50
20	4·71	2·73	2·76	0·33	0·63	0·47

in particular, for the sample containing 20% whiskers, without any distinction between the different whisker orientations. Because *D* is proportional to the crack roughness, it is evident that an increase in tortuosity and then, in crack deflection, causes a rise in fracture toughness for type $1_{//}$ cracks and in general, for the sample containing 20%SiC_w but not for type $1_\perp$ and $2_\perp$cracks.

By comparing all the results, it is evident that the improvement in toughness in type $1_{//}$ cracks, up to 6·1 $MPam^{0·5}$, is mainly connected to (i) the tortuosity, which increases as the whisker content increases, and (ii) the presence of high deviation angles. This crack geometry is a direct consequence of the microstructure, where the SiC-whiskers and the β-grains of Si_3N_4 have their axes perpendicular to the crack growth. It is interesting to note that high K_{IC} values are related to high deflection angles, in agreement with the experimental data reported by Willkens *et al.*,[27] showing that the fracture toughness of Si_3N_4–40%SiC_w samples increases as the angle between crack plane and whisker axis increases.

On the other hand, type $1_\perp$ or $2_\perp$ cracks are not very rough, with the exception of the 20%SiC_w composite, and present low deflection angles. For this direction, the mechanism of crack deflection is not very efficient to improve toughness. Only when the percentage of whiskers is high, 20%, does this mechanism appear to be more consistent.

For type $2_{//}$ cracks, the toughness increases as the percentage of whiskers increases, even though the tortuosity does not change. Other toughening mechanisms are involved, different from crack deflection, such as crack bridging,[28] which is not necessarily associated with an increase in roughness. More probably, in this direction crack bridging and crack deflection are both the dominant toughening mechanisms. When the SiC_w content increases up to 20%, the rise in the $(R_L)_0$ values indicates that the crack deflection mechanism has become predominant.

In Fig. 7, showing the K_{IC} values as a function of D_n, three different trends can be identified, depending on three different whisker orientations; only type $1_\perp$ or $2_\perp$ cracks obtained in the 20%SiC_w sample show a peculiar behaviour. These linear relationships seem to correspond to different crack geometries and different contributions of crack deflection, i.e. D_n discriminates between the fracture mechanisms involved.

In conclusion, the geometrical analysis of the crack profile provides quantitative information about the microstructural anisotropy of the samples, suggesting the most effective trajectory and the corresponding microstructure to improve toughness. The high values of K_{IC} are obtained when the crack deflection mechanism causes large deflection angles and tortuosity. These geometric peculiarities are present in particular when the

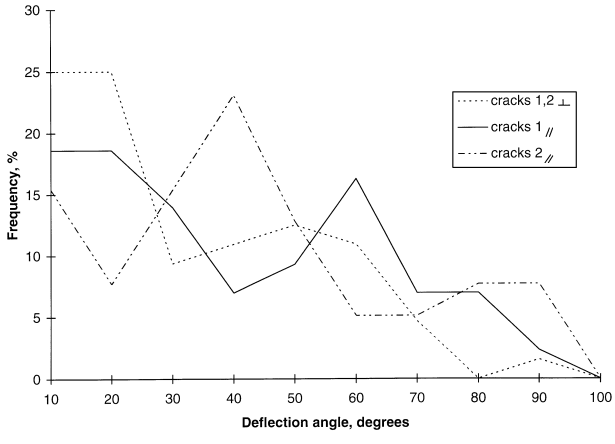

Fig. 5. Frequency of the deflection angles in the Si_3N_4-5%SiC_w sample.

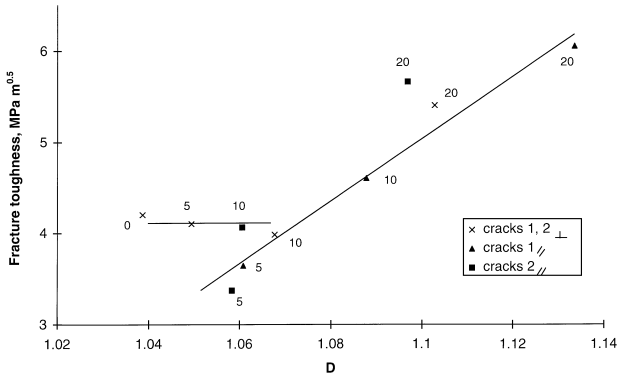

Fig. 6. Fracture toughness as a function of the fractal parameter *D*. The numbers in the plot represent the percentage of whiskers in the samples.

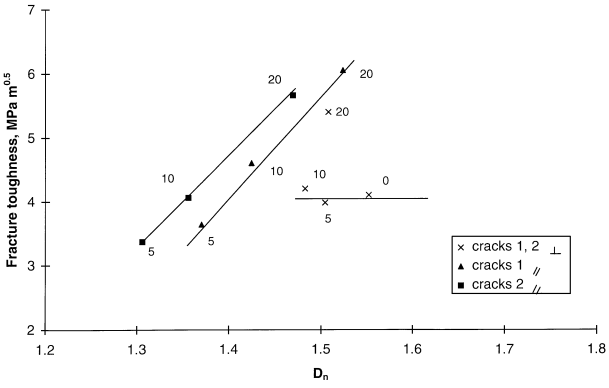

Fig. 7. Fracture toughness as a function of the fractal parameter D_n. The numbers in the plot represent the percentage of whiskers in the samples.

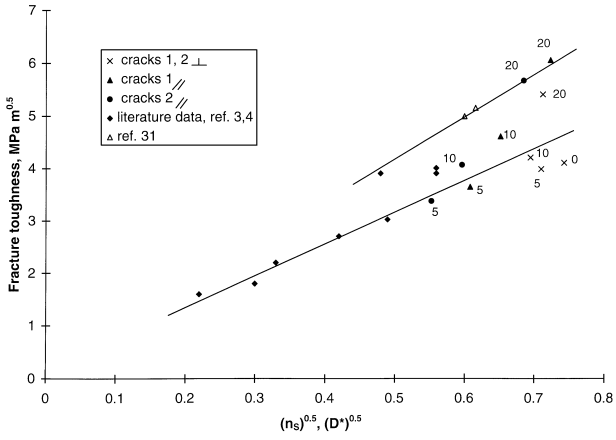

Fig. 8. Fracture toughness as a function of the fractal parameters n_s and D^*. The numbers in the plot represent the percentage of whiskers in the samples.

cracks grow perpendicularly to the whisker axis and the percentage of whiskers is 20%.

4.3 Geometry-energy correlation

The existence of a linear correlation between K_{IC} and surface fractal parameters, according to the relationship:

$$K_{IC} = K_0 + \left[E(a_0)^{0.5}\right] D^{*0.5} \qquad (11)$$

where E is the elastic modulus, a_0 is a characteristic length involved in the fracture process and D^* is the fractional part of the fractal parameter, has been reported in the literature.[3,4,12] According to eqn (11), the materials are divided into 'families' with the same value of $E(a_0)^{0.5}$. The presence of these classes of materials has been discussed in many papers and, in spite of some contradictions,[4,7] it seems useful to identify possible relationships between microstructure and mechanical properties. In particular, the slope of the straight line obtained in the plot K_{IC} versus $(D^*)^{0.5}$ allows one to calculate the a_0 value, that provides information on the fracture at the atomic level from data obtained with macroscopic observations.

The K_{IC} values of the tested Si_3N_4–SiC_w samples versus $(n_S)^{0.5}$ calculated using the eqn (10), are reported in Fig. 8 together with some data from the literature.[3,4] For these latter, the fractal parameter is D^*, determined directly on fracture surfaces using different experimental methodologies. It is interesting to observe that, for the samples tested in the present study, the general trend is that the K_{IC} increases as the fractal parameter increases in agreement with results reported in the literature.[3,4,12,29,30] Figure 8 shows that the samples containing 0,5 and 10%SiC_w belong to one of the 'families' of materials described in the literature, characterised by a fracture behaviour controlled by crack deflection. It is possible also to observe that the composite with 20% whiskers, characterised by the highest K_{IC} values, belongs to another 'family' of materials, together with two other composites of the zirconia-alumina system, analysed by the authors.[31]

The slope of the straight line characterising every family allows one to calculate the a_0 values: using the data of Young's modulus reported in literature,[19] a_0 results equal to 3 Å for 0, 5 and 10%SiC_w composites and 6 Å for 20% SiC_w. Mecholsky *et al.*[12] suggest that this atomic length a_0 is related to the breaking process that controls the fracture. For single crystals and polycrystalline materials, a_0 varies between 1 and 4 Å, a value of the order of the atomic radii. In this case the breaking of atomic bonds is the controlling process for fracture. For glass-ceramics, a_0 presents higher values, ranging between 20 and 70 Å. These lengths can be associated with the presence of molecular units like crystal clusters surrounded by glassy phases. The fracture energy γ_c, i.e. the energy/unit area required to form new crack surfaces, can be calculated using the relationship:[32]

$$\gamma_c = \frac{a_0 D^*}{2} E \qquad (12)$$

This equation is very significant because it relates the macroscopic fracture energy γ_c, to the atomic energy (Ea_0), through a geometrical parameter, D^* In the present case, the fracture energy can be evaluated on the basis of knowledge of the elastic modulus E and the geometrical parameters a_0 and n_S, obtained by the fractal analysis on crack profiles. Table 3 collects some results about energy–geometry relationships for different materials.[12,32]

The first five samples in Fig. 3 are characterised by low a_o values, 1–3Å, that correspond to the breaking of atomic bonds. In this case, the fracture

Table 3. Literature (ref. 12,32) and experimental data for fracture toughness, K_{IC}, fracture energy, γ_c, characteristic length involved in the fracture process, a_0, Young's modulus, E, and fractional part of the surface fractal parameter, D^*

Sample	K_{IC} ($MPam^{0.5}$)	γ_c (J/m^2)	a_0 ($\AA$)	E (GPa)	D*,n_s
CaF_2 (s.c)	0·39	0·5	1	114	0·07
Spinel (s.c)	1·3	3	3	240	0·09
Alumina AD90	3	11	3	390	0·21
Alumina AD999	4	19	3	406	0·31
Si_3N_4 + 0-5-10%SiC_w	3·4–4·6	15–25	3	317–329	0·3–0·5
Si_3N_4 + 20%SiC_w	5·4–6·1	50	6	339	0·5
Piroceram	2·8	25	20	120	0·17
Zinc-silicate MS 498-S	2	27	76	90	0·07
Zinc-silicate MS 500-4	2	27	53	89	0·12

energy necessary for cracks to grow is low and, therefore the toughness is low, depending on the E values. The other samples, instead, have higher a_0 values, up to 76 Å. This result means that the fracture process involves larger units, such as clusters. The fracture energy and, then, the toughness are higher because the microstructure of the materials is more resistance to fracture.

For the Si_3N_4–20%SiC_w sample, the a_0 value is slightly higher than for the other composites and the fracture energy shows a larger value for all the directions. In this case the microstructure seems to form a strong barrier to crack propagation. This conclusion is supported by microstructural observations on these samples by Backhaus-Ricoult *et al.*,[33] who identify the presence of agglomerates of whiskers that could be the cause of a more important degree of crack deflection. This result explains the peculiar behaviour of this sample in Figs 6 and 7. However, the similar values of a_0 found for all the composites analysed suggest that the breaking process at the atomic level could be always the same; probably a more thorough analysis of the microstructure of the samples would be useful to confirm the results obtained.

5 Conclusions

Fractal analysis of the crack geometry of different Si_3N_4-SiC_w composites has shown the potentiality of a quantitative approach in understanding the fracture mechanism in ceramic composites. The crack path appears to be a spectrum of the microstructure of the system and underlines the anisotropy of the materials, due to the orientation of the whiskers and β-grains of Si_3N_4.

Two parameters, the tortuosity R_L and the fractal dimension D_n of the cracks, reflect the importance of the crack deflection mechanism in improving toughness. Extrapolation of the fractal analysis of crack profiles to the corresponding fracture surface allows one to determine the length involved in the fracture process and the fracture energy. In the present study, this extrapolation showed that the high K_{IC} value found for the composite with 20%SiC_w could be due to the presence of clusters of whiskers. These results clearly indicate that the application of fractal analysis to the study of crack geometry in composite materials may well be an interesting technique to obtain a better understanding of the role that microstructure plays in the fracture process.

References

1. Mandelbrot, B. B., *Fractal: Form, Chance and Dimension*, W.H. Freeman, San Francisco, 1977.
2. Mandelbrot, B. B., Passoja, D. E. and Paulley, A. J., Fractal character of fracture surfaces of metals. *Nature*, 1984, **308**, 721–722.
3. Mecholsky, J. J., Passoja, D. E. and Feinberg-Ringel, K. S., Quantitative analysis of brittle fracture surfaces using fractal geometry. *Journal of American Ceramic Society*, 1989, **72**, 60–65.
4. Thompson, J. Y., Anusavice, K. J., Balasubramaniam, B. and Mecholsky, Jr. J. J., Effect of microcracking on the fracture toughness and fracture surface fractal dimension of lithia-based glass ceramics. *Journal of American Ceramic Society*, 1995, **78**, 3045–3049.
5. Chen, C. T. and Runt, J., Fractal analysis of polystyrene fracture surfaces. *Polymer Communication*, 1989, **30**, 334.
6. Bouchaud, E., Lapasset, G. and Planès, J., Fractal dimension of fractured surfaces: an universal value? *Europhysic Letters*, 1990, **13**, 73–79.
7. Baran, G. R., Roques-Carmes, C., Wehbi, D. and Degrange, M., Fractal characteristics of fracture surfaces. *Journal of American Ceramic Society*, 1992, **75**, 2687–2691.
8. Mosolov, A. B., Mechanics of fractal cracks in brittle solids. *Europhysic Letters*, 1993, **24**, 673–678.
9. Borodich, F. M., Some fractal models of fracture. *Journal of Mechanics and Physics of Solids*, 1997, **45**, 239–259.
10. Banerji, K., Quantitative fractography: a modern perspective. *Metallurgical Transactions A*, 1988, **19A**, 961–971.
11. Underwood, E. E. and Banerji, K., Quantitative fractography. In *ASM Handbook, Vol. 12, Fractography*. ASM International, 1992, pp. 193–210.
12. Mecholsky, J. J., Mackin, T. J. and Passoja, D. E., Self-similar crack propagation in brittle materials, In *Advances in Ceramics, Vol. 22, Fractography of Glasses and Ceramics*, eds, J. R. Varner and V. D. Frechette. 1988, pp. 127–134.
13. Buljan, S. T., Baldoni, J. G. and Huckabee, M. L., Si_3N_4-SiC composites. *American Ceramic Society Bullettin*, 1987, **66**, 347–352.

14. Unal, O., Petrovic, J. J. and Mitchell, T. E., Mechanical properties of hot isostatically pressed Si_3N_4 and Si_3N_4/SiC composites. *Journal of Material Research*, 1993, **8**, 626–634.
15. Campbell, G. H., Rühle, M., Dalgleish, B. J. and Evans, A.G., Whisker toughening: a comparison between aluminum oxide and silicon nitride toughened with silicon carbide. *Journal of American Ceramic Society*, 1990, **73**, 521–530.
16. Becher, P. F., Hsueh, C-H., Angelini, P. and Tiegs, T. N., Toughening behavior in whisker-reinforced ceramic matrix composites. *Journal of American Ceramic Society*, 1988, **71**, 1050–1061.
17. Underwood, E. E. and Banerji, K., Fractals in fractography. *Materials Science and Engineering*, 1986, **80**, 1–14.
18. Underwood, E. E. and Banerji, K., Fractal analysis of fracture surfaces. In *ASM Handbook, Vol. 12, Fractography*. ASM International, 1992, pp. 212–215.
19. Singh, J. P., Goretta, K. C., Kupperman, D. S., Routbort, J. L. and Rhodes, J. F., Fracture toughness and strength of SiC-whisker-reinforced Si_3N_4 composites. *Advanced Ceramic Materials*, 1988, **3**, 357–360.
20. Anstis, G. R., Chantikul, P., Lawn, B. R. and Marshall, D. B., A critical evaluation of indentation techniques for measuring fracture toughness: I, direct crack measurements. *Journal of American Ceramic Society*, 1981, **64**, 533–538.
21. Mandelbrot, B. B., *The Fractal Geometry of Nature*. W.H. Freeman, San Francisco, 1982.
22. Nemilov, S. V., *Thermodynamic and Kinetic Aspects of the Vitreous State*, CRC Press, Inc., Florida, 1995, pp. 119.
23. Russ, J. C., *Fractal Surfaces*. Plenum Press, New York, 1994.
24. Hamblin, M. G. and Stachowiak, G. W., Application of the Richardson technique to the analysis of surface profiles and particle boundaries. *Tribology Letters*, 1995, **1**, 95–108.
25. Becher, P. F. and Wei, G. C., Toughening behaviour in SiC-whisker-reinforced alumina. *Journal of American Ceramic Society*, 1984, C267-C269.
26. Lange, F. F., Relation between strength, fracture energy, and microstructure of hot-pressed Si_3N_4. *Journal of American Ceramic Society*, 1973, **56**, 518–522.
27. Willkens, C. A., Corbin, N. D., Pujari, V. K., Yeckley, R. L. and Mangaudis, M. J., The influence of microstructure orientation on the fracture toughness of Si_3N_4 based materials. *Ceramic Engineering & Science proceedings*, 1988, **9**, 1367–1370.
28. Fletcher, T. D., Petrovic, J. J. and Hack, J. E., Quantitative fractography of SiC whisker-Si_3N_4 matrix composites. *Journal of Materials Science*, 1991, **26**, 4491–4498.
29. Mecholsky, J. J. and Mackin, T. J., Fractal analysis of fracture in Ocala chert. *Journal of Materials Science Letters*, 1988, **7**, 1145–1147.
30. Issa, M. A., Hammad, A. M. and Chudnovsky, A., Correlation between crack tortuosity and fracture toughness in cementitious material. *International Journal of Fracture*, 1993, **60**, 97–105.
31. Celli, A., Tucci, A. and Esposito, L., unpublished results.
32. Passoja, D. E., Fundamental relationships between energy and geometry in fracture. *Advanced in Ceramics, vol. 22, Fractography of Glasses and ceramics* ed. J. R. Varner and V. D. Frechette 1988, pp.101–126
33. Backhaus-Ricoult, M., Castaing, J. and Routbort, J. L., Creep of SiC-whisker reinforced Si_3N_4. *Revue de Physique Appliquée*, 1988, **23**, 239–249.